THE DYNAMIC STALLING CHARACTERISTICS OF A RECTANGULAR WING WITH SWEPT TIPS

R.A.McD. Galbraith, F.N. Coton, D.Jiang, R. Gilmour
Department of Aerospace Engineering, The University of Glasgow, Glasgow,
G12 8QQ, U.K.

Abstract

This paper presents results from a test facility specifically designed to measure the pressure distributions on finite wings undergoing arbitrary pitching motions through dynamic stall. The main data presented in this paper are for a rectangular planform wing with swept tips instrumented with 192 miniature pressure transducers. Apart from describing the test facility, typical data from a series of high speed ramp-up motions to beyond stall are discussed. The data illustrate the three-dimensionality of the flow, and provide insight into the manner in which the tip vortices influence the development and subsequent convection of the dynamic stall vortex.

Nomenclature

c	chord
Cm	pitching moment coefficient
Cn	normal force coefficient
Cp	pressure coefficient
r	reduced pitch rate $\left(\dot{\alpha}c/2U\right)$
Re	Reynolds number
s	span
x	chordwise direction
y	direction normal to chord
z	spanwise direction
U	velocity
α	angle of attack
ω	rotational velocity

Introduction

It has been recognised for many years (1) that the maximum lifting force generated by a wing can be substantially enhanced if the wing is subject to rapid pitching motion. The detailed mechanisms which interact to produce this 'dynamic' effect, however, have still to be fully explained despite being of significance to both rotary-wing and fighter aircraft. Not surprisingly, therefore, much effort has been directed towards isolating the dominant flow mechanisms which influence the phenomenon. Of particular note are the works of McCroskey et al. (2), McAllister et al. (3) Petot (4) Wood (5) and Carta et al. (6) which have provided the foundations of contemporary understanding. In fact, on the basis of these works and several others, Young (7) was able to propose a good description of the characteristic phenomena associated with dynamic stall. A further notable review of progress in the field was later provided by Carr (8).

Despite these developments, many aspects of the dynamic stall process are still unclear. For example, two seemingly equivalent experiments (Lorber & Carta (9), Galbraith et al. (10)), pertaining to the effect of pitch rate on the convection velocity of the dynamic stall vortex, have yielded contradictory results. Green and Galbraith (11), who spent much effort assessing both the data sets involved, concluded that, if the geometric environments of the experiments were similar, the difference was most likely associated with the respective Mach numbers; 0.17 and 0.3.

For practical applications, a further complication arises from the strongly three-dimensional characteristics of many flow fields. The significance of this has been appreciated for some time, particularly with respect to stall cell development (12), but the difficulty in accurately measuring and interpreting three-dimensional flows restricted almost all the dynamic-stall tests noted above to nominally two-dimensional flow conditions.

In parallel with these experimental studies has been the development of semi-empirical dynamic stall models such as those of Beddoes (13), Lieshman & Beddoes (14), Gangwani (15) and Tran & Petot (16). Such models are predominantly two-dimensional and, although, as demonstrated by Beddoes (17), they can be coupled to an appropriate wake model to cope with the three-dimensional planform in the region of a helicopter blade tip, there are very little data available for comprehensive validation.

The tip region of helicopter blades has been further complicated by the emergence of new planforms including the so-called BERP tip. These tips can have highly swept leading edges which may produce fundamental differences between the stalling pattern at the tip and over the larger part of the rotor. The swept tip may be dominated, on the retreating side of the rotor disc, by a strong vortex similar to that of a delta wing, whilst the inner portions may be more akin to the two-dimensional test case. Thus, useful information on the complexities of the stall process may be obtained by isolating the differences between the dynamic stalling of a finite straight wing and that of a delta wing, and examining to what extent both associated phenomena interact for a straight wing with highly swept tips.

Improved understanding of these phenomena require the execution of three-dimensional dynamic stall experiments of which, to date, there are but a few. Of these, the majority have been motivated by aspects of fighter aircraft manoeuvrability and have thus considered only delta wings (18,19). A small number of tests have, however, been carried out on other wing planforms using a range of measurement techniques. The effect of wing sweep on the dynamic stall process was studied in detail by St. Hilaire and Carta (20) using an instrumented tunnel-spanning wing. In studies at the University of Colorado, flow visualisation, surface pressure measurement and hot wire anemometry was used to investigate the flow around oscillating cantilevered wing planforms (21,22). Some foresighted flow visualisation experiments were carried out at the same institution by Horner et al. (23) investigating both the manner of the stall and the associated connectivity of vortical structures. A more involved experiment was carried out by Pezali (24) at NASA Ames and involved a cantilevered finite wing heavily instrumented with pressure transducers.

For the past few years the authors have been developing a three-dimensional dynamic-stall facility to provide data on the effects of planform on the dynamic stalling process. To date, three finite wings have been tested in the facility; a straight planform (25,26) a delta wing and a straight wing with swept tips (27,28) at an angle equal to that of the delta wing.

This paper presents results from the test series conducted on the swept-tip wing. The data illustrate the three-dimensionality of the wing loading whilst exhibiting many of the features associated with nominally two-dimensional flow. Analysis highlights the role of the dynamic stall vortex and the influence which the wing tip vortices have on it is discussed.

Description of the Test Facility

The tests were carried out in the University of Glasgow's "Handley Page" wind tunnel which is a low-speed closed-return type. The wing model was located horizontally in its 2.13 × 1.61 metre octagonal working section and supported on three struts, as shown in Fig. 1. These were, in turn, connected to the main support structure and actuation mechanism situated below the tunnel. Movement of the model was produced by displacement of the two rear struts and the model was pivoted about the quarter chord position on a tool steel shaft connected to the front support via two self aligning bearings. The actuation force was produced using a Parker 2H Series linear hydraulic actuator and crank mechanism which allowed a variation of angle of attack from -26^{o} to 45^{o}. This system comprised the 2H series hydraulic cylinder, a bridge manifold, a high response proportional directional control valve with a E200-595 PID analogue closed loop controller and could deliver a maximum thrust of 17KN during extension and 6.53 KN during retraction at a piston speed of 1.1m/s. An angular displacement transducer mounted on the crank was used to provide a feedback signal and for recording the real time angle of attack.

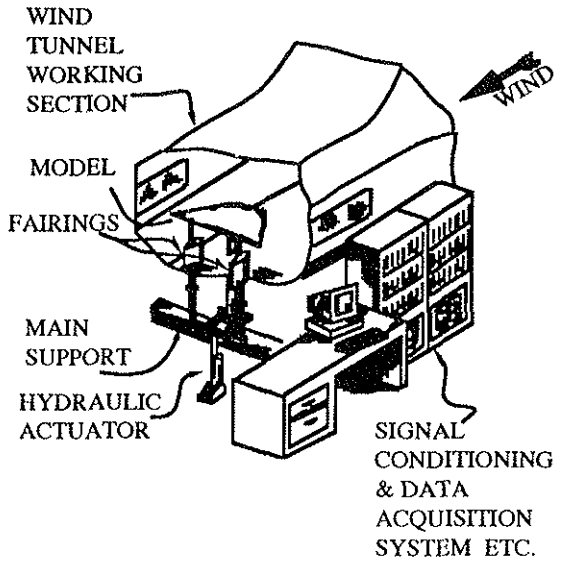

Fig. 1. Test set-up

The cross section of the wing was that of a NACA 0015 aerofoil. At the wing tips, the aerofoil profile shape was retained over approximately the first 15% of the chord and the intersection between the swept edge and the leading edge was rounded. On aft portions, the cross-sectional shape was tapered down to produce sharp leading edges. The model, of overall dimensions 126 cm x 42cm, was constructed with an aluminium framework of ribs and stringers with an outer epoxy glass fibre skin as shown in Fig. 2.

Altogether, 192 pressure transducers distributed on the upper and lower surfaces were placed within the model predominantly to the starboard side. On the swept-tip wing, three chordal arrays of 29 transducers were used on the main body of the wing. At the wing tip, a series of swept arrays, emanating from the virtual intersection of the leading edge and swept tip, were employed. The locations of the main transducer arrays on the upper surface of the model are illustrated in Fig. 2.

In order to check on the overall symmetry of the flow, three transducers were placed on the left side of the wing in corresponding positions to their counterparts on the starboard side. Additionally, three accelerometers were embedded in the wing, two of which were near the trailing edge on outboard locations and the final one was mounted centrally.

All pressure transducers were of Kulite differential type CJQH-187 with one side of the

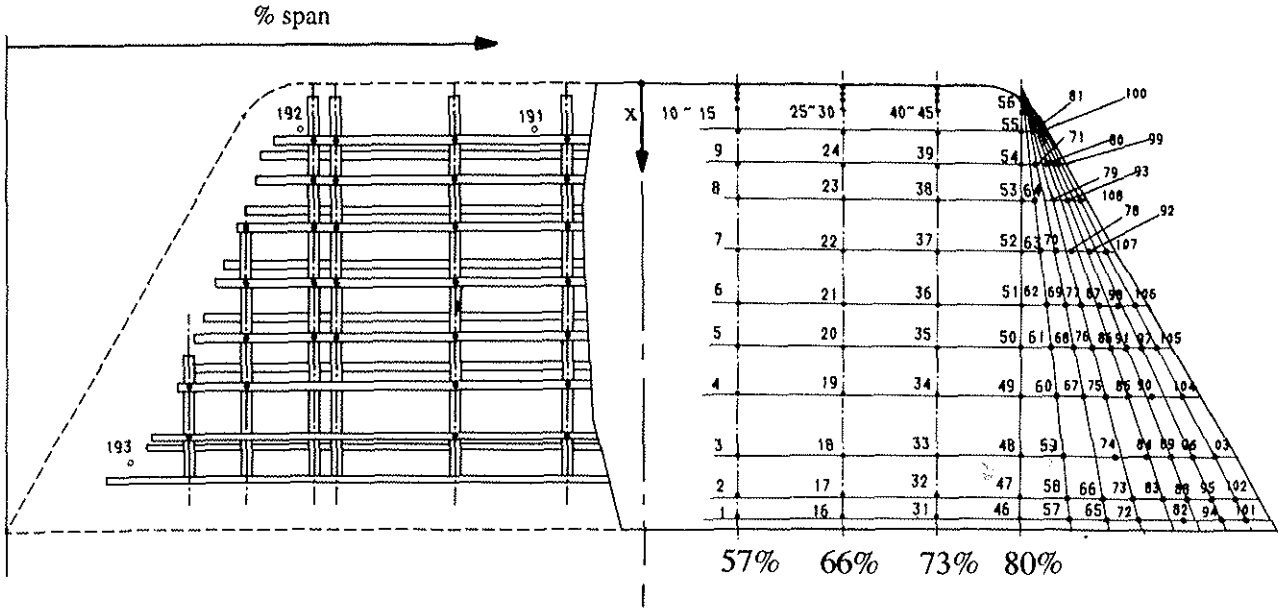

Fig. 2. Swept-tip wing model showing construction and upper surface transducer locations

pressure diaphragm open to the ambient pressure outside the wind-tunnel via tubing. The signals from all of the transducers were taken to a specially designed signal conditioning unit of modular construction with each module containing its own control board. On instruction from the computer, the control board automatically removed all offsets to below the A-D converter resolution and adjusted all gains as necessary. In fact, during a test, the computer sampled the maximum and minimum of each transducer output and adjusted the gains accordingly to improve the data acquisition resolution. The data acquisition was carried out by a PC microcomputer, configured with a 486 processor and interfaced with proprietary Bakker Electronics BE256 modules which provided the necessary analogue to digital conversion. The software used for data acquisition was TEAM 256. At present, the system has 200 channels, each of which is capable of sampling to a maximum rate of 50KHz, giving an overall sampling rate of 10MHz. A high sampling rate was required to capture the fine detail of the dynamic stall process, especially when the reduced pitch rates or reduced frequencies were relatively high.

The Test Sequence

For each wing studied in the research programme, four particular test motions were considered. The first of these was to assess the steady performance of the wing over an incidence range of -1.5^{o} to 43.5^{o}. Second, a sequence of ramp-up tests, in which the wing was pitched up at a constant rate, were conducted. For the lower pitch rates, excellent ramp functions were obtained but, as can be imagined, at the higher values the starting and stopping sequences induced non-linearities. Nonetheless, over the area of interest, i.e., stall initiation, the pitch rates remained relatively constant. Third, ramp-down tests in which the wing was subjected to a constant negative pitch rate were carried out and, finally, a series of oscillatory tests more typical of extant dynamic stall experiments were conducted.

Results

In this section, results from the swept-tip wing tests are presented in the form of pressure coefficient data together with force and moment coefficients obtained by integration of these data.

As indicated in the introduction, the tests on the swept-tip wing were the second part of a larger test programme involving three wing planforms. The data from the first test series, on a rectangular wing of aspect ratio three, were available for reference as were two-dimensional data for the NACA0015 aerofoil collected in a previous study (29). It was, therefore, possible to generate Fig. 3. where the wing normal force coefficient variation for the present model is compared with the other two cases for the static and a ramp-up test.

Clearly, the static data for the rectangular wing exhibit the classic effects of aspect ratio when compared to the nominally two-dimensional case. In particular, the gradient of the Cn curve and the severity of stall is reduced and the incidence of stall increased. Given that the swept-tip wing had the same overall dimensions as the rectangular wing, and hence a lower effective aspect ratio, it is not surprising that the gradient of its curve is even less and stall is further delayed until higher incidence.

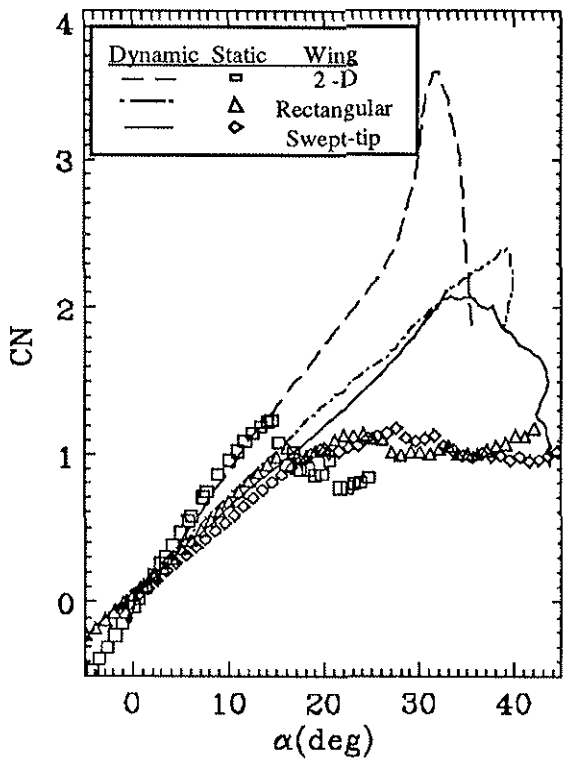

Fig. 3. Static and dynamic (r = 0.027) normal force coefficients for a two-dimensional aerofoil and two finite wings

The ramp-up data presented in the figure are for a relatively high reduced pitch rate, r=0.027, which corresponds to a linear reduced pitch rate in excess of 400^{o}/s. This case, however, provides a good illustration of the basic features of the general behavioural trends witnessed in the all of the ramp up tests. Specifically, the fundamental influence of aspect ratio on the gradient of the linear portion of the curves is once again clearly visible. It should be noted, however, that the gradients are not identical to the static cases. In fact, whilst the dynamic response lags the static curve in the two-dimensional case, the opposite is true for the two finite wings. Irrespective of this, in all three cases the linear portion of the dynamic curve is extended well beyond its static equivalent and, as a result, the peak Cn is much greater. In the nominally two-dimensional case, this is heightened by a sharp increase in the gradient of the curve prior to stall. There is very little evidence of this in the rectangular wing results whereas the swept-tip wing exhibits a progressively increasing Cn gradient as stall is approached. Interestingly, however, stall occurs earlier on the swept-tip wing than on the rectangular wing.

The pitching moment coefficients for the same cases are presented in Fig. 4. Once again, the static data display the fundamental effects of aspect ratio. In particular, the build up in Cm prior to pitching moment stall is clearly absent in the case of the two finite wings. Instead, a steady decrease in Cm is observed, presumably as a consequence the suppression of leading edge suction and the localised aft loading in the region of the wing tips. In the high pitch rate case there is a sharp downturn in the two-dimensional pitching moment trace at around 22^{o}. Similar changes in Cm occur on the two finite wings but, in both cases, the break occurs later and is much less severe.

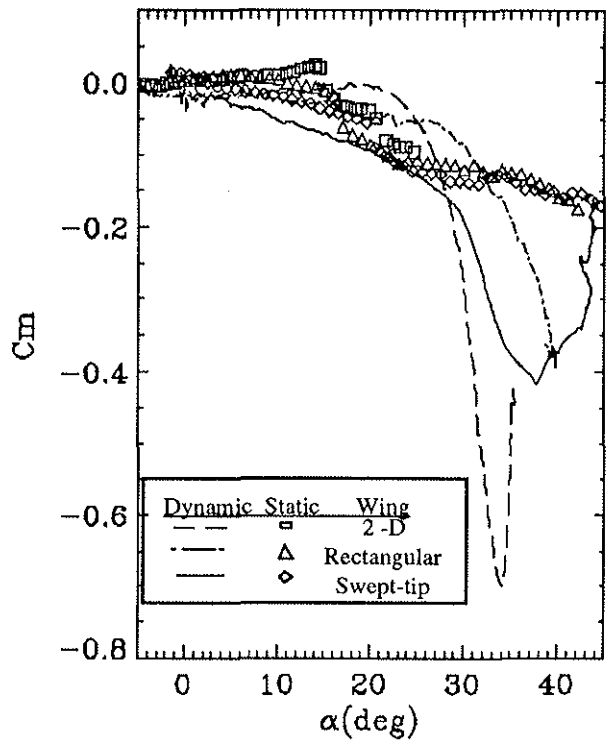

Fig. 4. Static and dynamic (r = 0.027) pitching moment coefficients for a two-dimensional aerofoil and two finite wings

The influence of pitch rate on the normal force produced by the swept-tip wing can be clearly observed in Fig. 5. In the figure, four pitch rate cases, ranging from r=0.011 to r=0.027, are compared to their static counterpart for a linear ramp between -1.5^{o} to 43.5^{o}. Most noticeable is the progressive overshoot of static stall as the pitch rate is increased. In addition, the Cn corresponding to a given geometric incidence also increases with pitch rate. This appears to be a consequence of an initial impulsive jump in Cn coupled with an enhanced rate of growth.

As indicated in the previous section, the arrangement of pressure transducers on the swept-tip wing was such that there were four chordwise arrays inboard of the wing tips. Integration of the measurements taken at these span positions allowed local force and moment coefficients to be evaluated.

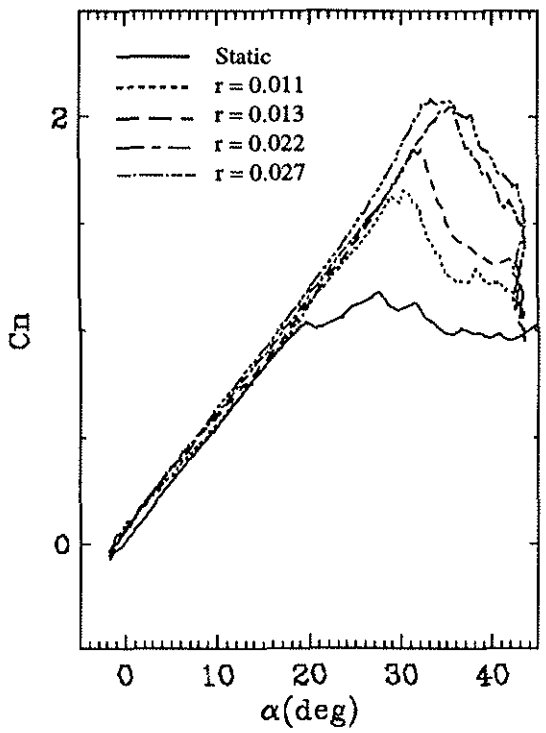

Fig. 5. The effect of pitch rate on the normal force coefficients for the full swept-tip wing

The effect of pitch rate on the normal force coefficients at each of these four spanwise locations is presented in Fig. 6.

At 57% of span, the effect of increasing pitch rate at low to moderate incidence is similar to that witnessed on the full wing. Once again, Cn stall is progressively delayed and, consequently, the peak value attained is observed to increase with pitch rate. This increase is not, however, monotonic with the peak values for the two highest pitch rate cases being almost identical. A final important feature of this figure is the lack of a substantial increase in the gradient of the curves prior to stall which, as noted in Fig. 3. is one of the classic hallmarks of two-dimensional low-speed dynamic stall. There is evidence of a small increase in gradient prior to stall at the higher pitch rates but this is much less than for two-dimensional flow and is very short lived.

Similar behaviour to that described above is observed at 66% of span. In this case, however, the rise in Cn prior to stall is much more pronounced at higher pitch rates and the corresponding peak values are significantly enhanced. The results from the two highest pitch rate cases are very similar although the highest Cn value is achieved at r=0.022.

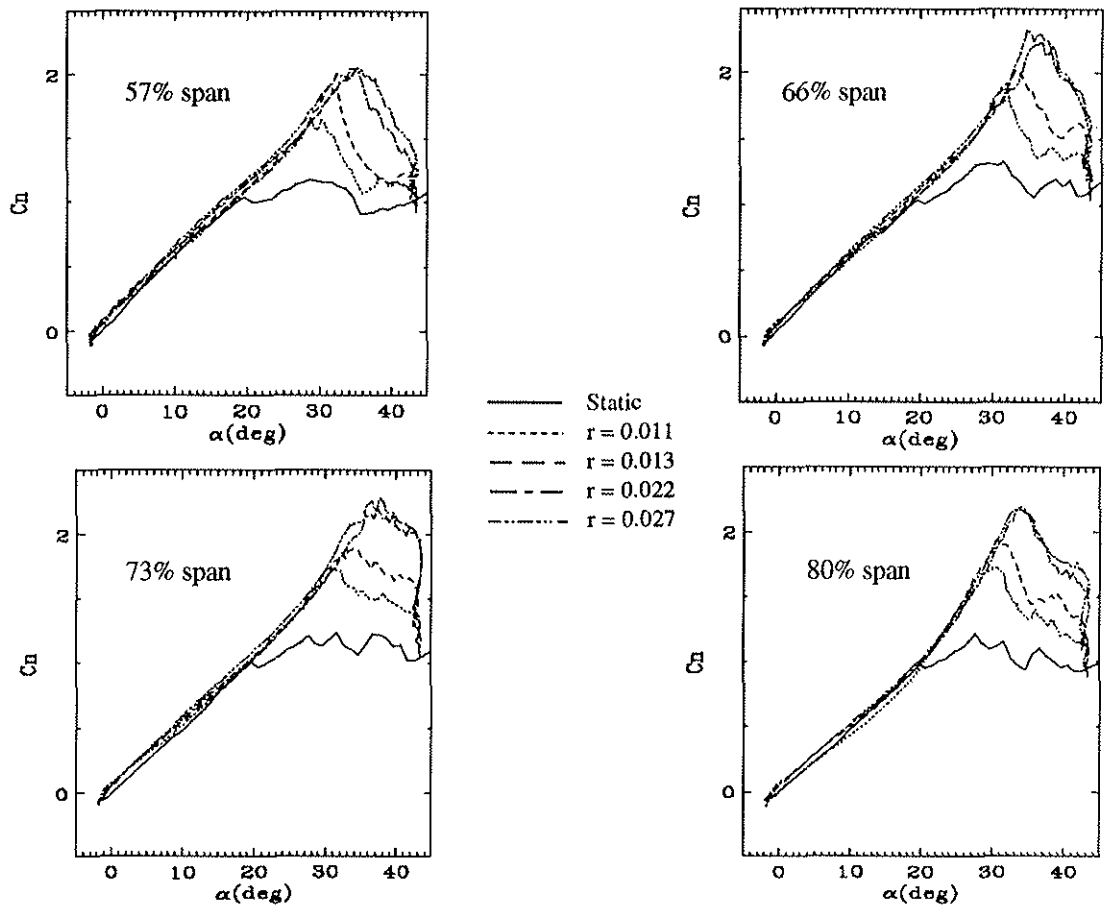

Fig. 6. The effect of pitch rate on the normal force coefficients at four spanwise locations

At 73% of span the initial gradients of all the Cn curves are marginally higher than in the previous two cases. Most of the basic features are, however, the same as the 66% of span location although the peak Cn values are generally lower and the stall is less severe.

The final spanwise position, 80%, is located at the intercept of the swept tip and the leading edge. Despite this proximity to the wing tip, the peak Cn values are comparable to the previous cases. The main feature which distinguishes these results from those in the other three plots is the progressive increase in Cn gradient with increasing incidence. In fact, despite a low initial rate of Cn growth, the gradients of the curves prior to stall are well in excess of those observed on inboard sections of the wing. An immediate consequence of this is an earlier stall than in the previous cases.

The quarter chord pitching moments produced by the wing at the different pitch rates are presented in Fig. 7. All the dynamic cases exhibit a progressive downward trend in Cm with the initial gradients depending on the pitch rate. As in the corresponding Cn plot, Fig. 5, the coefficients overshoot the static values by a margin which increases with pitch rate.

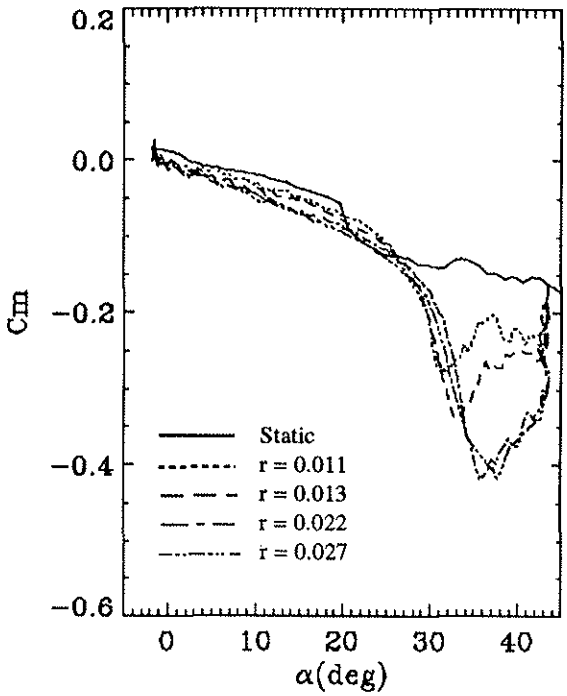

Fig. 7. The effect of pitch rate on the pitching moment coefficient for the full swept-tip wing

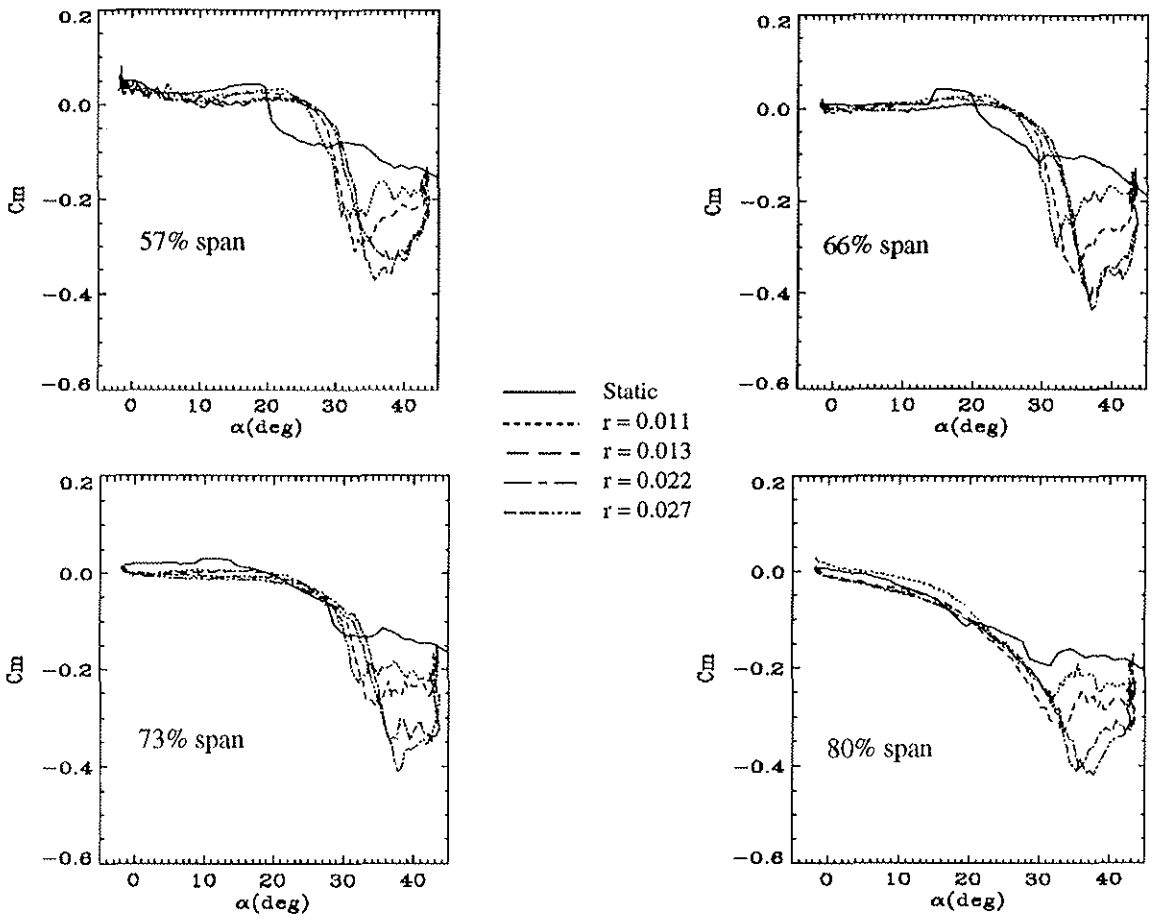

Fig. 8. The effect of pitch rate on the pitching moment coefficients at four spanwise locations

Figure 8 presents the local quarter chord pitching moment coefficients corresponding to the normal force curves presented in Fig. 6. At 57% of span, the static pitching moment exhibits a steady build-up towards stall followed, at around 22°, by a rapid decrease as the pitching moment becomes strongly nose-down. Subsequently, the pitching moment becomes progressively more negative as the incidence is increased further. With increasing pitch rate, the build up in Cm at moderate incidence is reduced and the pitching moment break is delayed. This break also becomes less well defined as the pitch rate increases. It should be noted that the break occurs prior to Cn stall and is most severe at incidences which correspond to the increased Cn gradient in Fig. 6. Once it occurs, however, its extent, and hence the magnitude of the peak nose-down moment, increases with increasing pitch rate. Finally, all the curves tend towards the steady bluff-body state. It is interesting to note that both the static curve and the data corresponding to r = 0.027 are very similar to their nominally two-dimensional counterparts presented in Fig. 7.

At 66% of span, the initial values of all the curves are considerably lower than the previous case although the peak Cm values are almost identical. At around 14°, the static curve exhibits an abrupt rise which may be associated with the development of stall cells on the wing. The post moment stall behaviour of all the curves is broadly in line with the previous case although higher peak nose-down moments are measured in all dynamic cases.

Further outboard, at 73% of span, the initial values of the pitching moment are very similar to those at 66% of span. Once again, the gradient of Cm, prior to the moment break, is observed to depend on pitch rate. In fact, by r = 0.022 the Cm gradient becomes negative. As in the previous case, the static curve exhibits some small-scale abrupt changes but, this time, these occur earlier between 9° and 14°. The subsequent decrease in the value of Cm is also initiated earlier at around 15° and is much more gradual than in the previous two cases. The dynamic data also exhibit a more gradual break in Cm but the peak nose-down values achieved are quite similar to those at 66% of span.

The final plot of Fig. 8. presents the pitching moment coefficients measured at 80% of span. Here, there is little evidence of a clear break in Cm but, rather, the curves all display an almost monotonic downward progression. Consequently, Cm values are generally lower than all the previous cases and, with the exception of the highest pitch rate case, the peak nose-down values occur at lower incidence and are of greater magnitude.

Further clues to the nature of the flow development can be obtained by examination of the span-wise temporal pressure distributions at various chordal locations. These are presented in Fig. 9., for the r = 0.027 pitch rate case, at three chordal locations. As an aid to interpretation, the data from the instrumented half of the wing has been reflected on to the opposite side giving a full span appearance that is symmetric about the mid-span position.

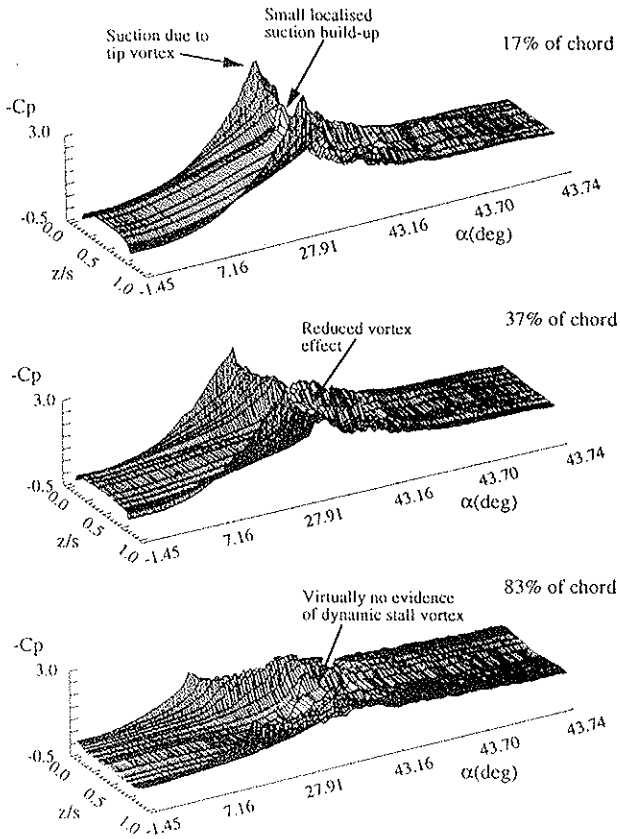

Fig. 9. Variation of spanwise upper surface pressure distribution with incidence at three chordal locations (r = 0.027)

At 17% of chord, the spanwise pressure profile builds up steadily as the incidence increases up to approximately 7°. Beyond this, the growth in suction on inboard sections continues steadily whilst, at the tips, rapid increases in suction, which subsequently dominate the loading distribution, are observed. Nevertheless, a key feature appears between 57% and 66% of span just prior to the collapse of the wing tip suction. Here, as indicated in the diagram, there is a small but rapid increase in local suction. Temporally, this increase is short lived but there is some evidence of chordwise convection since it also appears briefly at 37% of chord. Near the trailing edge, apart from the suction build up at the wing tips, the pressure profiles are relatively featureless.

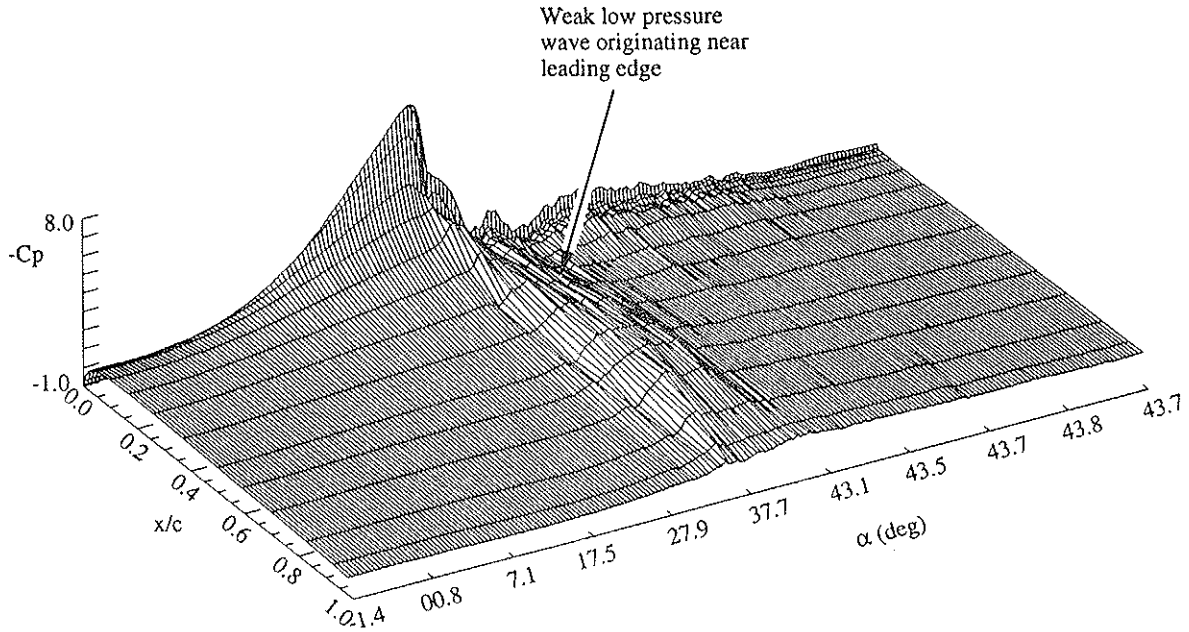

Fig. 10. Variation of chordwise upper surface pressure distribution with incidence at 66% of span (r = 0.027)

Figure 10 shows the upper surface chordwise pressure distribution at 66% of span plotted against incidence. In this figure the disturbance identified above is clearly visible as a low pressure wave which originates behind the leading edge suction peak and subsequently convects rearwards. During its progression downstream, the wave becomes less distinct to the extent that there is almost no evidence of its passage over the trailing edge.

Discussion

Contemporary understanding of the complex series of events which contribute to the phenomenon of low speed dynamic stall is based predominantly on experience of nominally two-dimensional flows. In the absence of three-dimensional effects, it has been possible to isolate and, hence, identify the basic features of the stall process and, using this information, to subsequently develop semi-empirical dynamic stall models. These models have found application in a wide range of unsteady aerodynamics applications but, invariably, have been combined with other aerodynamic schemes which represent the three-dimensional geometry of the particular problem. For a wing, this implies that the primary inception and stall development processes are essentially the same in three-dimensions as in two, and are only modified by the gross induced flow generated by the wing tip vortices. If this is the case, the phenomena observed in the present test series may be explained by reference to basic wing theory and current understanding of nominally two-dimensional dynamic stall.

Although the exact mechanism of dynamic stall vortex inception in two-dimensional flow is still unclear, the overall process prior to and after vortex formation is well documented. In particular, it is known that the suppression of trailing edge separation during the pitching motion leads to an extension of Cn growth beyond the point of static stall, with higher pitch rates producing a larger overshoot. Subsequently, if the reduced pitch rate is high enough, a strong 'dynamic stall' vortex forms near the quarter chord location and grows in strength before travelling rearwards over the aerofoil. This vortex produces a localised area of increased suction on the upper surface of the aerofoil which is, in turn, responsible for the increase in Cn gradient and the sharp downwards break in Cm identified in Figs. 3 and 4. As the vortex moves rearwards, the leading edge suction peak collapses and Cn stall occurs.

The basic behaviour described above is evident in much of the data presented for the swept-tip wing. In fact, the Cn data presented in Figs. 5 and 6 all exhibit an overshoot of their static counterparts which depends on reduced pitch rate. In Figs. 7 and 8, the pitching moment stall is also similarly delayed. As stall is approached, the formation of a dynamic stall vortex is indicated by the increase of the Cn gradient in Fig. 6 at 66% and 73% of span, at high pitch rates, and the corresponding sharp breaks in Cm in Fig. 8. Further evidence of the existence of a vortex, in the highest pitch rate case is found in Fig. 9. as a localised suction build up, and in Fig. 10, as a low pressure ridge.

It may have been expected that the strongest manifestation of the dynamic stall vortex would be at 57% of span where the influence from the wing tips is least. Curiously, however, there is very little evidence of a rise in the Cn gradient here, except at the highest

pitch rate. It is also interesting to note that, in terms of the full wing, the integrated Cn curves presented in Fig. 5 show no clear effects of a vortex.

In steady flow, finite wings exhibit a spanwise loading distribution as a consequence of the modification to the onset flow by the downwash from the tip vortex systems. The effect of the downwash, which is strongest near the wing tips, is to reduce the effective incidence across the wing. As may be expected, therefore, the extent of the wing which is subject to this effect depends mainly on the aspect ratio. In fact, for low aspect ratio wings, such as the current test model, almost the entire wing exhibits the hallmarks of the downwash effect. A clear illustration of this is evident in the steady Cn data presented in Fig. 3 where the gradient of the linear portion of the normal force curve is significantly higher in the nominally two-dimensional case than for the two finite wings. Indeed, the Cn curve for the swept tip wing, which has the lowest effective aspect ratio, exhibits the smallest gradient. An inevitable consequence of this behaviour is the progressive delay of stall as the aspect ratio reduces.

When a finite wing is subject to pitching motion, such as in the present case, the temporal change in loading gives rise to shed vorticity. This is also true in the nominally two-dimensional case where the shed vorticity acts to reduce the effective incidence experienced by the aerofoil. As shown in Fig. 3., at high pitch rates this has the effect of reducing the Cn produced at a given geometric incidence on the linear portion of the curve. It could, therefore, be anticipated that the vorticity shed from the finite wings would act in the same manner but, conversely, the dynamic Cn response is observed to lead the static data. The explanation for this lies not in the shed vorticity effect but, rather, in the temporal development of the tip vortices.

As a wing is pitched, the total strength of the trailed tip vortices at any instant in time depends on the history of the wing loading. Thus, at a given geometric incidence during a ramp-up, downstream segments of the tip vortex structure are weaker than those close to the wing. The integrated effect of this vorticity distribution will, therefore, be less than the corresponding static case where the strength of the tip vortex is effectively constant in the streamwise direction. Consequently, the downwash produced at a given geometric incidence during the pitching motion will be weaker than that at the static equivalent. The corresponding higher effective incidence, therefore, accounts for the lead in the dynamic Cn response of the finite wings observed in Fig. 3. The progressive effect of increasing pitch rate is also clear in Fig. 5.

The above discussion does not, however, explain the apparent absence of the dynamic stall vortex from the mid span region. In fact, on the basis of the above, it would be expected that the vortex would be strongest and, hence, most obvious at the 57% of span location. Clearly, the spanwise development of the vortex is highly three dimensional and may be more directly influenced by the tip vortices than simply via an induced incidence effect. The behaviour of the two vortex systems will now be examined in more detail.

Dynamic Stall Vortex

Valuable information on the formation and subsequent development of the dynamic stall vortex on a finite wing has been obtained in two recent flow visualisation studies (23,30). In the first of these, Horner et al. examined the development of vortical structures on a pitching flat plate whilst, in the second, Coton and Moir examined the flow around scale models of the wings used in the present study. On both the flat plate and the rectangular wing model the dynamic stall vortex was observed to form almost uniformly along the span. This observation was supported by pressure measurements on the rectangular wing (31) which indicated that the first tangible sign of vortex formation, Cp deviation, occurred uniformly over most of the span. The subsequent development of the vortex was, however, observed to be highly three-dimensional. In fact, the portion of the vortex near the mid span was found to grow faster than outboard sections and to lift upwards as it did so. The resulting flow structure, termed an omega vortex, is illustrated in Fig. 11. This structure then convected rearwards, establishing connectivity with the tip vortices near the mid span.

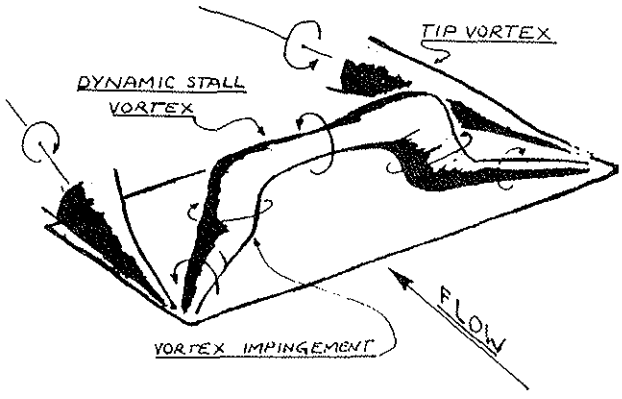

Fig. 11. Sketch of the 'omega' vortex system observed on a pitching rectangular wing

The flow visualisation studies of the swept-tip wing found that the dynamic stall vortex generally behaved similarly to the rectangular wing case. Unfortunately, testing limitations made it difficult to determine the spanwise uniformity of the initial development of the vortex. Once formed, however, the vortex was clearly visible and the latter stages of its development, in which its central portions rise above the wing, are clearly shown in the sequence of

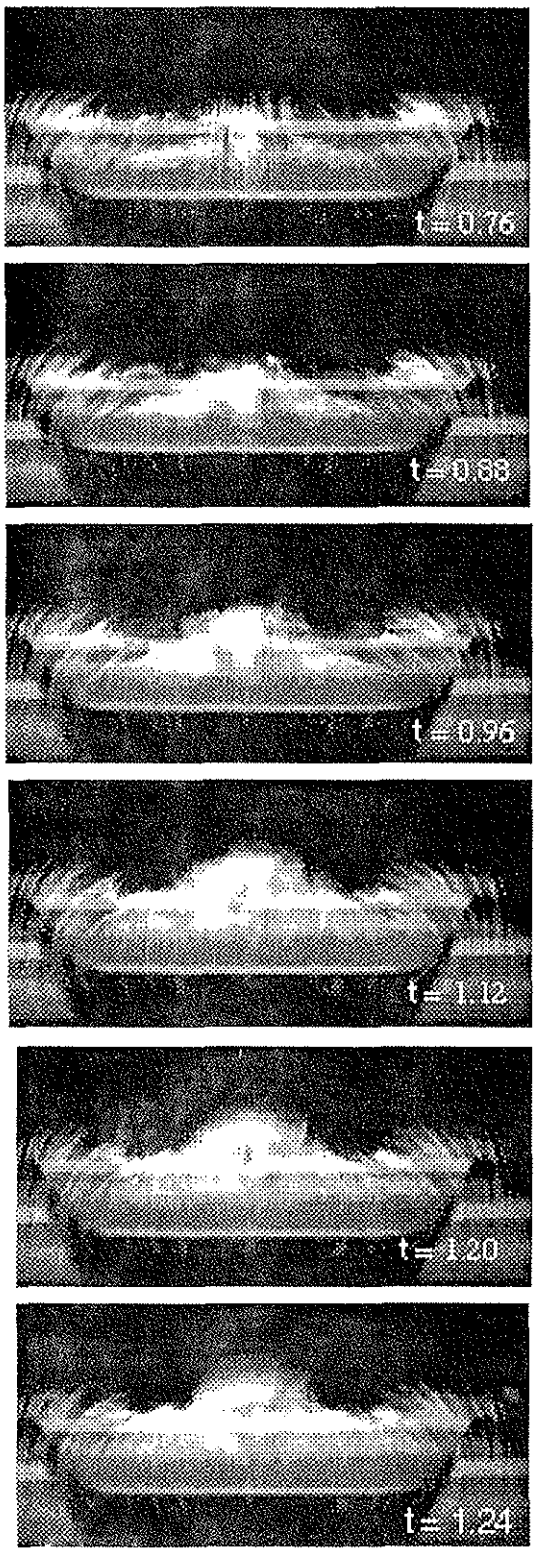

Fig. 12 Smoke flow images collected on a swept-tip wing pitching during the latter stages of a ramp-up from 0 to 40 degrees (Re = 13,000, r = 0.08)

photographs presented in Fig. 12. for a high reduced pitch rate ramp-up test. Interestingly, however, the omega vortex structure was found to occupy a smaller portion of the span than its rectangular wing counterpart and its central portion was apparently raised higher above the wing.

It should be noted that, despite the large difference in Reynolds number between the present test series and the flow visualisation studies, experience suggests that the same basic flow features will be present in both cases. This allows many of pressure features identified earlier to be more fully explained. It is likely that the build up of the wing loading is initially dominated by the downwash from the wing tips. This reduces the local effective incidence progressively as the wing tips are approached and accounts for the different Cn gradients observed at different spanwise stations in Fig. 6. The reduction in effective incidence delays dynamic stall onset but the associated reduction in effective reduced pitch rate acts in the opposite sense. On the rectangular wing it was found that these two effects appear to be balanced and vortex inception occurs simultaneously across the span (31). On the present wing, detailed analysis of the pressure histories indicate that vortex inception occurs earlier at the mid span. This is possibly due to the orientation of the wing tip vortices with respect to the planform, but further analysis of this effect is required.

Once formed, the vortex continues to grow giving rise to the local increase in suction near the leading edge identified in Figs. 9 and 10 at 66% of span. This, in turn, produces the change in the gradient of the local Cn shown in Fig. 6. The lack of spanwise uniformity of the vortex is then heightened by more rapid growth at the mid-span than on outboard sections. This would be expected to produce a strong surge in Cn at around 57% of span but no such effect is visible. This is because the weaker segments of the vortex near the tip are forced downwards towards the surface by the tip vortices and, at the same time, the central sections of the vortex lift from the surface to form the so-called 'omega' structure. As these central portions lift away, the localised suction produced by them diminishes. Conversely, the suction produced by the impingement of the vertical legs of the 'omega' vortex on the surface is much more significant. On this particular wing, this appears to occur somewhere between 66% and 73% of span and is the reason for the suction ridge observed in Fig. 10. The rearward convection of these vertical 'legs' is also the reason for the severe Cm break at these spanwise locations.

On this particular wing, the flow visualisation studies indicated that the central portions of the vortex struggled to maintain coherence and finally broke up above the wing. This may explain the lack of evidence for vortex convection from the trailing edge.

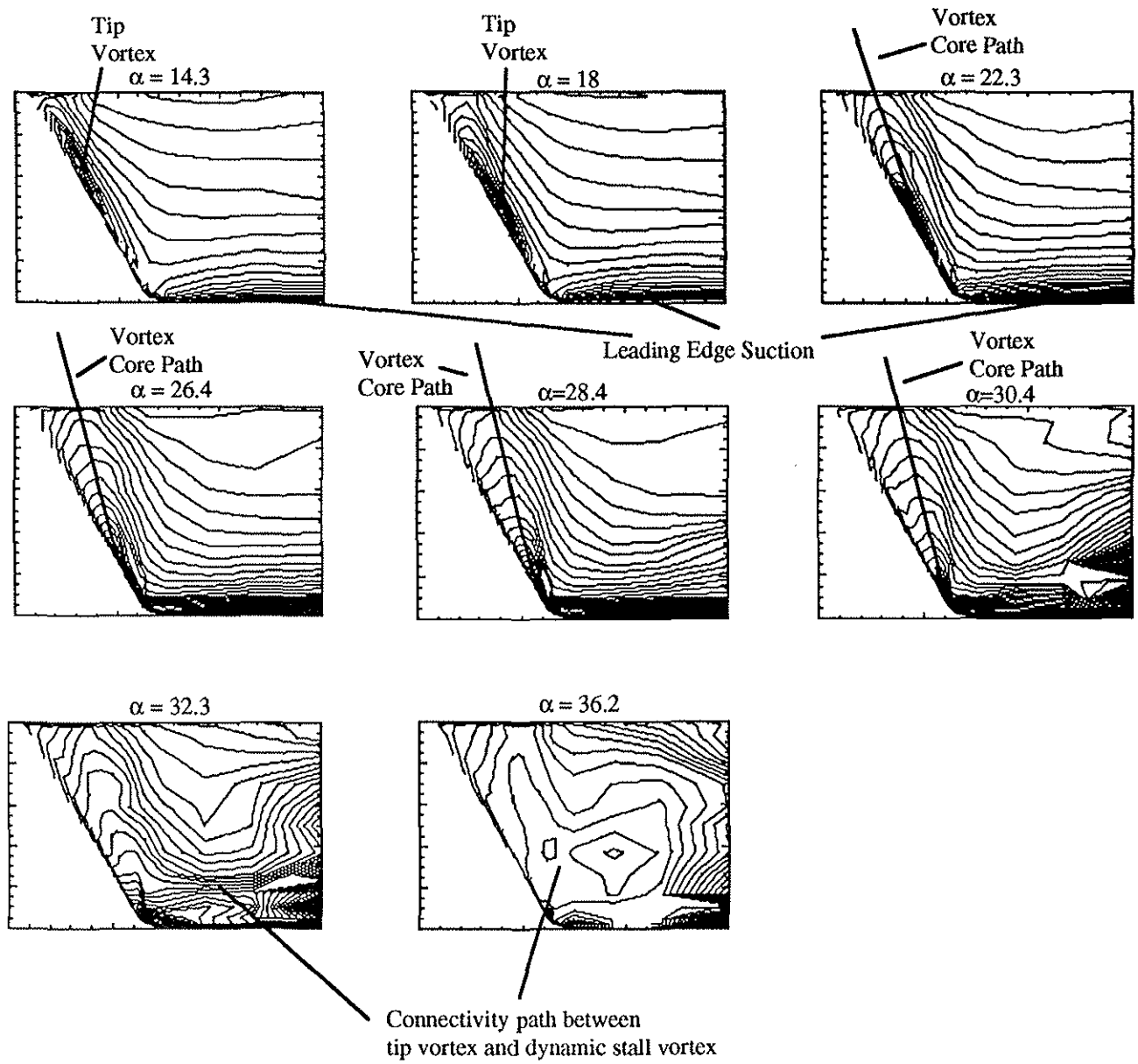

Fig. 13. Illustration of surface loading patterns via pressure contours at eight different angles of attack during a ramp-up motion (r = 0.027).

Wing Tip Vortices

Throughout the build-up of the dynamic stall vortex, there is a corresponding increase in the strength of the tip vortices. Initially, the cores of these vortices are located on aft portions of the wing tip but, as the incidence is increased, they move steadily forwards. The timing of these events with respect to geometric incidence depends very much on the reduced pitch rate. For the highest pitch rate case, r=0.027, their forward progression is illustrated in Fig. 13 where contour plots showing the qualitative distribution of pressure at different incidence values are presented. It is interesting to note that the behaviour of the vortices is not identical to those on a delta wing which tend to originate from the wing apex. Neither is it identical to the rectangular wing where the suction from the vortices is confined to aft portions of the wing.

Once the vortex core has reached the region of the leading edge, however, its manifestation becomes very similar to that of a delta wing vortex. At this point, the core path swings rapidly inboard but its effect weakens as it does so. This is clearly illustrated in Fig. 14 which shows the pressure histories for

transducers located at different spanwise locations on the swept-tip at 50% of chord. Up to 23°, the highest suction values are measured on the transducer closest to the wing tip. There is then a progressive decay of suction from the wing tip inwards as the vortex core changes its position and weakens. By 30°, the core is much broader and has moved well inboard. Total collapse of the tip vortex follows shortly afterwards.

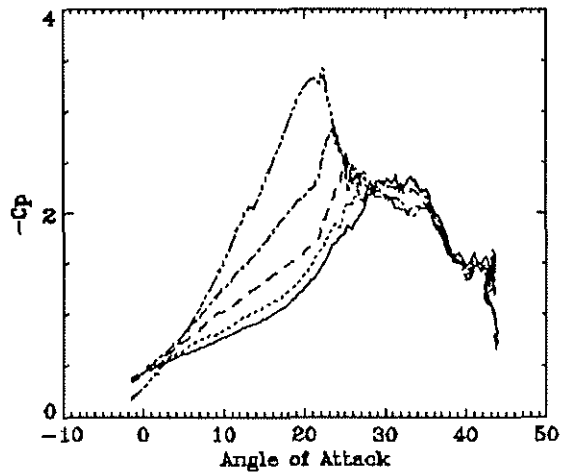

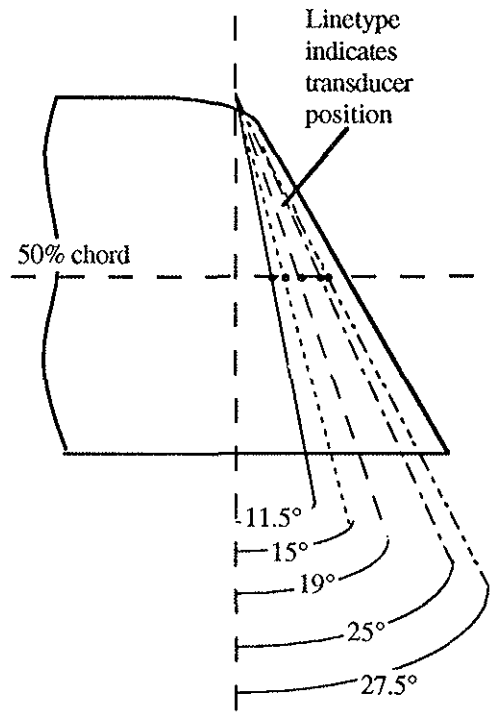

Fig. 14. Variation of surface pressures with incidence on the swept tip. (x/c = 0.5)

At this point, it is interesting to note in Fig. 13 that the inward movement of the tip vortex is accompanied by some subtle changes in the pressure distribution on inboard sections of the wing. Given that dynamic stall vortex inception occurs at around 28° at the mid span, and slightly later on outboard sections. It seems likely that the movement of the tip vortex may be a factor in this process.

In the latter stages of the flow development, the tip vortex becomes clearly connected to the stall vortex by the path highlighted in Fig. 13 at 32°. Connectivity is then maintained until the collapse of the vortex structures.

Conclusions

Results from surface pressure measurement tests on a pitching swept-tip wing have been presented. The data illustrate the fundamental features of the wing loading and, together with flow visualisation results, provide insight into the flow mechanisms present on the wing. Evidence was found of a dynamic stall vortex which, in the presence of the tip vortex system, appeared to distort significantly. The development of these two vortex systems was examined in some detail and the extent to which they interact was explored.

Acknowledgements

The work was carried out with funding from the Engineering & Physical Science Research Council, (Grant Ref. SERC GR/H48330) Westland Helicopters, Defence Research Agency and the University of Glasgow. The authors acknowledge with gratitude the help and support of their sponsors.

References

(1) Harper, P.W., Flanigan, R.E., 'The effect of change of angle of attack on the maximum lift of a small model', NACA TN-2061, 1950

(2) McCroskey,W.J, and Fisher, R.K. ' Detailed aerodynamic measurements on a model rotor in the blade stall regime', AIAA Journal, Vol. 17, No.1, pp 20-30, 1972.

(3) McAlister, K.W., Carr,L.W.,and McCroskey, W.J. ' Dynamic stall experiments on NACA0012 airfoil', NACA TP-1100, 1978

(4) Petot, J.J., ' Experimental and theoretical studies on helicopter blade tips at ONERA', 6th European Rotorcraft and Powered Lift Aircraft Forum, Bristol, 1980

(5) Wood,M.E., ' Results of oscillatory pitch and ramp tests on the NACA0012 blade section', ARA Memo No. 220, December, 1979

(6) Carta,F.O., ' Experimental investigation of the unsteady aerodynamic characteristics of a NACA 0012 airfoil', Res. Rep. M-1283-1, United Aircraft Corp., July,1960

(7) Young,W.H.,Jr,' Fluid mechanics mechanisms'. NASA -TM- 81956, March 1981

(8) Carr, L.W., 'Progress in analysis and prediction of dynamic stall', Journal of Aircraft, Vol. 25, No. 1., January 1988

(9) Lorber,R.F., Carta,F.O., 'Unsteady stall penetration experiments at high Reynolds number', AFOSR TR-87-1202, UTRC R87-956939-3, 1987

(10) Galbraith,R.A.McD, Gracey, M.W. and Leitch, E., 'Summary of pressure data for thirteen aerofoils on the University of Glasgow's aerofoil database', G.U. Aero Report: 9221, 1992.

(11) Green,R.B,Galbraith,R.A.McD, Niven,A.J.,' Measurements of the dynamic stall vortex convection speed', The Aeronautical Journal of The Royal Aeronautical Society, October 1992

(12) Moss,G.F., Murdin,P.W., ' Two dimensional low-speed tunnel tests on the NACA 0012 section including measurement made during pitch oscillations at the stall', RAE Technical Report CP No. 1145, 1968

(13) Beddoes,T.S., 'Representation of airfoil behaviour', AGARD Specialists Meeting on the Prediction of Aerodynamic Loads on Rotorcraft, AGARD CP-334, 1982, also Vertica, Vol. 7, (2)., 1983

(14) Leishman,J.G., Beddoes,T.S., ' A semi-empirical model for dynamic stall', Journal of The American Helicopter Society, July 1989

(15) Gangwani,S.T., ' Synthesised airfoil data method for prediction of dynamic stall and unsteady airfoils', Proceedings of the 39th Annual Forum of the America Helicopter Society, 1983, also Vertica, Vol. 8, 1984

(16) Tran,C.T., Petot,D., ' Semi-empirical model for the dynamic stall of airfoils in view of the application to the calculation of responses', ONERA T.P. 103-1980.

(17) Beddoes,T.S., ' A 3-D separation model for arbitrary planforms', 47th Annual Forum of the American Helicopter Society, Phoenix, Arizona, May 1991

(18) Gad-el-Hak, M., Ho., C-M., 'The pitching delta wing', AIAA Journal, Vol. 23, No. 11, Nov. 1985

(19) Thompson, S.A., Batill, S.M., Nelson, R.C., 'Delta wing surface pressures for high angle of attack maneuvres', AIAA Atmospheric Flight Mechanics Conference, Oregon, 1990

(20) St. Hilaire, A.O., Carta, F.O., ' Analysis of unswept and swept wing chordwise pressure data from an oscillating NACA 0012 airfoil experiment', Vol.1 - Technical Report, NASA CR-3567,1983

(21) Ashworth, J., Huyer, S., Luttges, M., 'Comparisons of unsteady flow fields about straight and swept wings using flow visualization and hot-wire anemometry', AIAA 19th Fluid Dynamics, Plasma Dynamics and Lasers Conference, Hawaii, 1987

(22) Ashworth, J., Crisler, W., Luttges, M., 'Vortex flows created by sinusoidal oscillation of three-dimensional wings', AIAA 7th Applied Aerodynamics Conference, Seattle, 1989

(23) Horner,M.B., Addington, G.A., Young III, J.W. and Luttges, M.W., 'Controlled Three-Dimensionality in Unsteady Separation Flows about a Sinusoidally Oscillating Flat Plate', AIAA- 90-0689, Jan. 1990

(24) Piziall, R.A., ' 2-D and 3-D Oscillating Wing Aerodynamics for a Range of Angles of Attack Including Stall', NASA-TM-4632, September 1994

(25) Jiang, D., Coton, F. N., Galbraith, R.A.McD., Gilmour, R.,' Collected data for tests on a NACA 0015 section rectangular wing (aspect ratio 3)', Vols. 1 - 8, G.U. Aero. Repts 9515 - 9522, 1995

(26) Galbraith, R. A. McD., Coton, F. N., Jiang, D., Gilmour, R., 'Preliminary results from a three-dimensional dynamic stall experiment of a finite wing', 21st European Rotorcraft Forum, St. Petersburg, Russia, 1995

(27) Jiang, D., Coton, F.N., Galbraith, R.A.McD., Gilmour, R. , ' Collected data for tests on a NACA 0015 section rectangular wing with 60^{o} swept tips.', Vols. 1 - 8, G.U. Aero. Repts 9527 - 9534, 1995

(28) Galbraith, R.A.McD., Coton, F.N., Jiang, D., Gilmour, R. ' The comparison between the dynamic stall of a finite wing with straight and swept tips', International Congress of the Aerospace Sciences, Sorrento, Italy, 1996

(29) Angell, R.K. Musgrove, P.J. and Galbraith, R.A.McD. 'Collected Data for tests on a NACA 0015 aerofoil.', Vols 1, 2 & 3, G.U. Aero Report 8805, 1988.

(30) Moir, S., Coton, F.N., 'An examination of the dynamic stalling of two wing planforms', G.U. Aero. Report 9526, 1995

(31) Coton, F.N., Galbraith, R.A.McD., Jiang, D., Gilmour, R., 'An experimental study of the effect of pitch rate on the dynamic stall of a finite wing', Conference on Unsteady Aerodynamics, The Royal Aeronautical Society, London, 1996